Evaluation of a reduced pressure chemical ion reactor utilizing adduct ionization for the detection of gaseous organic and inorganic species

Matthieu Riva[1,2, †,*], Veronika Pospisilova[1,†], Carla Frege[1], Sebastien Perrier[2], Priyanka Bansal[1], Spiro Jorga[1], Patrick Sturm[1], Joel A. Thornton[3], Urs Rohner[1], Felipe Lopez-Hilfiker[1,*]

[1] TOFWERK, 3645 Thun, Switzerland

[2] Université Claude Bernard Lyon 1 CNRS, IRCELYON 69626, Villeurbanne France

[3] Department of Atmospheric Sciences, University of Washington, Seattle, Washington 98195, USA.

Correspondence to: matthieu.riva@tofwerk.com & lopez@tofwerk.com

[†] These authors contributed equally.

Abstract

Volatile organic compounds (VOCs) and volatile inorganic compounds (VICs) provide critical information across many scientific fields including atmospheric chemistry, soil, and biological processes. Chemical ionization (CI) mass spectrometry has become a powerful tool for tracking these chemically complex and temporally variable compounds in a variety of laboratory and field environments. It is particularly powerful with time-of-flight mass spectrometers, which can measure hundreds of compounds in a fraction of a second and have enabled entirely new branches of VOC/VIC research in atmospheric and biological chemistry. To accurately describe each step of these chemical, physical, and biological processes, measurements across the entire range of gaseous products is crucial. Recently, chemically comprehensive gas-phase measurements have been performed using many CI mass spectrometers deployed in parallel, each utilizing a different ionization method to cover a broad range of compounds. Here we introduce the recently developed Vocus AIM (Adduct Ionization Mechanism) ion-molecule reactor (IMR), which samples trace vapors in air and ionizes them via chemical ionization at medium pressures. The Vocus AIM supports the use of many different reagent ions of positive and negative polarity and is largely independent of changes in the sample humidity. Within the present study, we present the performance and explore the capabilities of the Vocus AIM using various chemical ionization schemes, including Chloride (Cl^-), Bromide (Br^-), Iodide (I^-), Nitrate (NO_3^-), Benzene cations ($C_6H_6^+$), Acetone dimers (($C_3H_6O)_2H^+$), and Ammonium (NH_4^+) reagent ions primarily in laboratory and flow tube experiments. We report the technical characteristics, operational principles, and compare its performance in terms of time response, humidity dependence, and sensitivity to that of previous chemical ionization approaches. This work demonstrates the benefits of the Vocus AIM reactor which provides a versatile platform to characterize VOCs and VICs in real time at trace concentrations.

1. Introduction

Mass spectrometry represents a nearly universal method for determining the chemical composition of organic and inorganic species across various environmental matrices. In the fields of environmental and atmospheric chemistry, chemical ionization (CI) is a versatile real-time method to measure individual organic and inorganic compounds in air at trace concentrations (Yuan et al., 2017; Riva et al., 2019; Zhang W. et al., 2023; Zhang Y. et al., 2023). As in all chemical ionization systems, trace analytes in air react with excess reagent ions, leading to the formation of charged product ions usually via electron/proton transfer or adduct formation (Zhang W. et al., 2023; Zhang Y. et al., 2023). Advances in the field of chemical ionization over the last decade have yielded exceptionally low detection limits down to 10^4 molecules cm^{-3} (part-per-quadrillion), expanded dynamic ranges, and the capability of measuring a wide range of gaseous organic and inorganic species with time resolutions of up to 50 Hz (Riva et al., 2019; Zhang W. et al., 2023; Zhang Y. et al., 2023).

Chemical ionization mass spectrometers are uniquely able to measure temporal variability of trace VOC and atmospheric oxidation products; both in the laboratory and in the field, providing a critical tool to mechanistically track the most important atmospheric oxidation processes (Hallquist et al., 2009, Ehn et al., 2014, Bianchi et al., 2019). In particular, CI has made enormous improvements in the detection and quantification of reactive gaseous oxygenated species, including peroxy (RO_2) radicals, stabilized Criegee intermediates, and inorganic acids and bases which are difficult to directly detect with any other available analytical technique (Berndt et al., 2015, 2017, 2018; Breitenlechner et al., 2017; Hansel et al., 2018; Krechmer et al., 2018). For example, measurements via chemical ionization mass spectrometry (CIMS) have been pivotal in discovering the existence and importance of extremely low volatility organic molecules (ELVOCs). These compounds are now understood to be formed ubiquitously in the atmosphere and are critical to new particle formation and growth (Ehn et al., 2014; Bianchi et al., 2019). As a result, CIMS has emerged as a core analytical tool in atmospheric chemistry and related fields which require high sensitivity, high temporal resolution, and molecular-level speciation (Bruderer et al., 2019; Riva et al., 2019; Tang et al., 2019; Mazzucotelli et al., 2022; Zhang W. et al., 2023; Zhang Y. et al., 2023).

67   With the right selection of reagent ions, CI offers the possibility of soft, selective, and sensitive

68   online detection, for essentially any class of chemical compounds. While in practice, no reagent ion can

69   simultaneously detect the entire distribution of volatile compounds present in the atmosphere with sufficient

70   selectivity and sensitivity, different reagent ions can be selected to target distinct chemical families

71   (Crounse et al., 2006; Bertram et al., 2011, 2016; Lee et al., 2014, Bianchi et al., 2019, Riva et al., 2019;

72   Zhang W. et al., 2023; Zhang Y. et al., 2023). Therefore, a critical choice for chemical ionization operators

73   is which reagent ion is best suited to measure compounds of interest in each measurement scenario.

74   Recent advancements in the design of the reactor have sought to improve measurement quality by

75   addressing two outstanding limitations of chemical ionization mass spectrometers: (i) improved detection

76   efficiency by refining the reactor geometry and optimizing the flow dynamics within the system, and (ii)

77   reliable, reproducible, and fully controlled reaction conditions. Improvements in the detection efficiency

78   depend on the balance of two critical parameters in any chemical ionization reactor. First, compounds

79   present in the sample gas stream need to be efficiently transported to the reaction cell and mix/react with

80   the reagent ions. The efficiency of the first step depends primarily on ionization pressure and absolute flow

81   rate (i.e., residence time). At atmospheric pressure, gases diffuse slowly, and maintaining laminar flows

82   between the sample line and reaction cell is straightforward (e.g., Eisele-inlet, MION, Crossflow CIMS)

83   (Eisele and Tanner, 1993; Palm et al., 2019; Rissanen et al., 2019, Pfeifer et al., 2020). However, operating

84   at high pressure makes controlling ionization conditions much more challenging. Therefore, most CIMS

85   instruments operated at a reduced pressure to facilitate control of the ionization conditions. Sample vapors

86   enter most reduced-pressure chemical ionization mass spectrometers through a critical orifice, which

87   introduces turbulence as the gas expands into the reaction cell. These turbulences can introduce contact

88   between the neutral sample gas and the reactor walls, resulting in memory effects and losses of reactive

89   trace compounds by collision with the walls. While there have been numerous efforts to improve the

90   introduction of sample gases into reduced pressure reactors by laminarizing (Palm et al., 2019) the incoming

91   airflow or controlling the expansion inside of specially coated glass tubes (Vasquez et al., 2018), these

92   approaches are often complex and demand considerable optimization, which has hindered their widespread

93   adoption. Consequently, turbulent wall losses and memory effects continue to pose substantial challenges

94   in reduced-pressure chemical ionization instruments, particularly when detecting reactive or sticky

95   compounds.

96   Operating chemical ionization instruments at reduced pressure provides more refined control over

97   ion chemistry since it allows for more straightforward and effective manipulation of ions within the

98   instrument. Of particular nuisance in nearly all chemical ionization approaches is water vapor, which is

99   highly variable and can have significant effects on the chemical ionization process. The formation of water

100   clusters, which grow rapidly as a function of increasing pressure, presents a specific challenge for

101   measurements taken near atmospheric pressure. Even chemical ionization approaches that operate at low

102   pressures like proton transfer reaction (PTR) can be affected by the presence of water vapor (Yuan et al.,

103   2017). PTR instruments are widely used for the detection of trace VOC using high electric fields to control

104   the reagent ion populations under changing humidity. While PTR instruments can largely control the

105   ionization and collision conditions in the reactor, applying high electric fields results in extensive

106   fragmentation of some critical functional groups in many fields (Yuan et al., 2017). Further, the PTR

107   ionization process is well known to lead to significant fragmentation of labile compounds such as acids,

108   peroxides, and alcohols. The fragmentation induced by protonation or charge transfer reactions along with

109   elevated collision energy within the reactor significantly complicates the mass spectrum, in some cases

110   limiting the possibility of retrieving the accurate concentration and composition of many classes of

111   compounds including highly oxygenated and functionalized organic species.

112   To improve the sensitivity (specificity) and reduce the degree of fragmentation, softer chemical

113   ionization techniques relying on adduct formation have become increasingly popular, especially when

114   molecular identification and mechanistic pathways must be accurately tracked. These reactors operate under

115   low (E/N <10 Td) or field-free conditions at pressures (typically 50-500 mbar), to promote adduct formation

116   and stabilization (Zhang W. et al., 2023; Zhang Y. et al., 2023). Fluid dynamics and the degree of turbulence

117   inside the reactor govern reaction times and ion transport in such reactors. At these elevated ionization

118   pressures, the effect of water vapor can become a critical parameter affecting sensitivity. Routinely used

119 reagent ions can result in order of magnitude changes in sensitivity under atmospherically relevant

120 fluctuations of humidity (Lee et al., 2014; Breitenlechner et al., 2017; Zhang W. et al., 2023; Zhang Y. et

121 al., 2023). Correcting the data for each compound's humidity dependence is an error-prone and time-

122 consuming process where each compound must be treated essentially individually. Flooding the reactor

123 with water vapor, as done in techniques like Vocus PTR, can suppress the humidity dependence of some

124 compounds. Such approaches are only applicable to certain groups of compounds whose water vapor

125 dependence becomes weaker at higher absolute concentrations of water, which is not a universal

126 characteristic. In general, the lack of adequate water vapor control remains a major drawback of chemical

127 ionization systems most critically those operated at pressures greater than 10 mbar.

128 Herein we introduce the Vocus AIM ion molecule reactor (IMR) and report the technical

129 characteristics, operation principle, and performance of this new chemical reactor. We evaluate its

130 performance by reporting the time response of nitric acid, demonstrating a novel approach to suppress

131 humidity dependence, and comparing sensitivity to other CI reactors. We present the design and capabilities

132 of the Vocus AIM using a wide variety of reagent ions, including Chloride (Cl^-), Bromide (Br^-), Iodide (I^-

133), Nitrate (NO_3^-), Benzene cations ($C_6H_6^+$), Acetone dimers (($C_2H_5O)_2H^+$), and Ammonium (NH_4^+) ions.

134 Finally, we show the measurement of RO_2 radicals and oxygenated VOCs acquired during the proof-of-

135 concept experiment of OH/O_3-initiated oxidation of α-pinene. This work highlights the benefits of the

136 Vocus AIM reactor within atmospheric chemistry and its limitations.

137 **2. Experimental Section**

138 2.1. Vocus AIM Reactor Design

139 Medium pressure chemical ionization (20-500 mbar) systems are typically designed as flow tube reactors

140 which primarily transport ions toward the reactor exit by gas flow. Manipulating ions at high pressure would

141 require high electric fields which are either impractical or could fragment the labile analyte ions. Further,

142 RF devices that could focus ions into a beam, do not efficiently operate at such high pressures, precluding

143 their efficient use. Therefore, the Vocus AIM reactor operates on many of the same fundamental principles

144 of more traditional flow tube reactors, including field-free ionization conditions (Figure 1) and fluid

145 dynamic transport of ions through the reactor. Specifically, the new design includes improvements in

146 sample and reagent ion introduction, a conductive polytetrafluoroethylene (cPTFE) Teflon conical reaction

147 chamber to improve time response, and a simple yet efficient quadrupole based differentially pumped TOF

148 interface.

149   Gases enter the reactor manifold via a ½" O.D. Swagelok fitting which is pumped through an inlet

150 via a radially symmetric pump port. Excess flow is used to maintain short residence time and to minimize

151 inlet memory effects such as surface reaction (conversion) and irreversible wall losses. Typical make-up

152 flow rates of 5-10 standard liters per minute (slpm) are used to transport neutral analytes efficiently to the

153 entrance of the reactor. A bored through Swagelok interface ensures that all wetted surfaces before the

154 reactor are Teflon®, to minimize the retention and memory of the inlet line for semi-volatile gases and

155 reduce surface activity. At the entrance of the Vocus AIM IMR, the sample flow enters directly into the

156 center of the conical reactor at a flow rate of 1.8 slpm through a stainless-steel critical orifice (0.475 mm)

157 and a PFA Teflon® sample flow guide which promotes subsampling from the center of the laminar inlet

158 flow. The reactor is typically operated at a pressure of 50 mbar as a compromise between sensitivity and

159 linear range and is controlled by a pressure control valve and an IDP3 vacuum pump (Agilent Technologies,

160 IDP3). The reactor is temperature controlled to 50 ˚C, which is the lowest temperature that can be reliably

161 controlled across various field conditions to ensure constant reaction conditions. While a lower reactor

162 temperature would promote adduct formation, the long-term stability of thermal conditions would be more

163 difficult to maintain. Reagent ions are generated by compact Vacuum Ultra-Violet (VUV) ion sources

164 arranged radially around the central axis with reactant ions injected at an angle (45 degrees) to intersect the

165 expanding sample flow with minimal sample deflection and ensure that no VUV light directly enters the

166 IMR. Each ion source introduces the ions into the reactor with a standard flow rate of 0.25 slpm for optimum

167 reagent ion yield (Figure S1), nearly an order of magnitude lower flows than polonium or X-ray based ion

168 sources typically used. The residence time inside the reactor under these standard conditions is ~ 10 ms.

169   Modeled flow velocities in the Vocus AIM IMR (Figure 1) were used to optimize the flow patterns

170   inside the reaction cell. The velocity field shows the intersection of the reagent ion jet with the sample flow

171   and was optimized to minimize the contact of sample gas with reactor surfaces as well as to prevent

172   turbulent eddies near the gas expansion region. The gas flow dynamics were modeled with the open-source

173   computational fluid dynamics (CFD) software OpenFOAM v8 (https://openfoam.org/) using a customized

174   solver (https://github.com/pasturm/rhoReactingPimpleFoam) to simulate supersonic flow in a vacuum with

175   mixing of different gases. The final geometry is constrained by machinability (finite tool dimensions) while

176   also minimizing the response time and reducing reactive and ion wall losses.
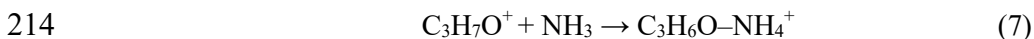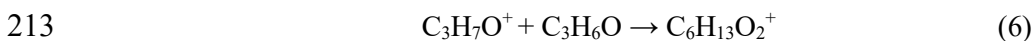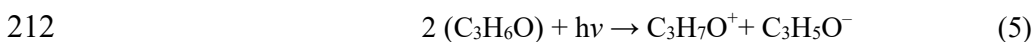
177   2.2 Reagent Ion Generation

178   Compact VUV ion sources generate reagent ions by converting photons from a VUV lamp (UV Lamp

179   Krypton DC PID PKS 106, Hereaus) at two wavelength bands corresponding to energies of ~10.0 and 10.6

180   eV into the desired reagent ions (Ji et al., 2020; Breitenlechner et al., 2022). As in prior work, we utilize a

181   primary photo-absorber (e.g., benzene) as a source of photoelectrons and directly formed cations to generate

182   subsequent reagent ions. Permeation tubes are held at 80 °C in a compact oven and deliver constant amounts

183   of corresponding photo-absorber and reagent ion precursor into the 0.250 slpm UHP nitrogen stream.

184   Gaseous benzene (C_6H_6, Sigma Aldrich, ≥99.9%) delivered from the permeation tube, enters the VUV lamp

185   housing and is photoionized (with an absorption cross-section of 4 x10^{17} cm^2 molecule^{-1} and ionization

186   potential = 9.24 eV), yielding $C_6H_6^+$ and photoelectrons (Lavi et al., 2018). By mixing benzene with trace

187   methyl iodide (CH_3I, Sigma Aldrich, 99.8%), bromoethane (C_2H_5Br, Sigma Aldrich, ≥99%) or nitric acid

188   (HNO_3, Sigma Aldrich, ≥65.6%), various anions such as I^-, Br^-, or NO_3^- are generated alongside with $C_6H_6^+$

189   following reactions equations (1 and 2) and are introduced into the Vocus AIM reactor. The compatibility

190   between multiple ion chemistries in the AIM system is determined by whether a generated reagent ion can

191   detect the neutral precursors from any other attached ion source. A small aperture at the exit of the

192   illuminated region of the ion source prevents back-diffusion of sample air into the primary ionization

193   chamber.

194 $$C_6H_6 + h\nu \rightarrow C_6H_6^+ + e^- \qquad (1)$$

195 $$CH_3I + e^- \rightarrow CH_3 + I^- \qquad (2)$$

196 By manipulating the above mechanisms, other reagent ions can be readily produced in high abundance and

197 high purity. Cl^- reagent ions can also be produced by introducing 0.250 slpm of UHP nitrogen through the

198 permeation tube oven containing pure dichloromethane (CH_2Cl_2, Sigma Aldrich, $\geq$99.8%) permeation tube.

199 Once formed, anion reagent ions mix with the sample flow in the main reaction chamber and ionize the

200 compounds of interest (M) through the reactions described in equations (3 and 4), with X being I^-, Br^-, Cl^-

201 or $(HNO_3)_nNO_3^-$ (n = 0,1,2).

202 $$M + X^- \rightarrow M^{\cdots}X^- \qquad (3)$$

203 $$M + X^- \rightarrow M\text{-}H^- + HX \qquad (4)$$

204 To generate ammonium ions, we irradiate gaseous acetone with VUV light, which results in self-protonated

205 acetone (5) and directly reacts with the acetone molecules yielding protonated acetone dimers (6) (Dong et

206 al., 2022). A continuous flow of NH_3, typically a few sccm, (i.e., $[NH_3] > 100$ ppm) from a 1% gas cylinder

207 (in nitrogen) can be introduced directly into the VUV source along with the acetone (Figure 1), NH_3

208 molecules react with the protonated acetone yielding acetone-ammonia adducts which can be used for

209 subsequent ionization in the main reaction chamber (7). If the concentration of NH_3 is lower than 100 ppm,

210 multiple ionization processes might occur (e.g., acetone dimers, charge transfer,...) which would

211 complicate the mass spectrum analyses.

212 $$2\,(C_3H_6O) + h\nu \rightarrow C_3H_7O^+ + C_3H_5O^- \qquad (5)$$

213 $$C_3H_7O^+ + C_3H_6O \rightarrow C_6H_{13}O_2^+ \qquad (6)$$

214 $$C_3H_7O^+ + NH_3 \rightarrow C_3H_6O\text{--}NH_4^+ \qquad (7)$$

215 Similar to anion reagent ions, these positive ions can ionize the compounds of interest through either adduct

216 formation or proton transfer or in the case of benzene, charge transfer. At pressures of 50 mbar, most

217 chemical ionization reactions occur via ligand switching reactions involving the analyte and hydrated

218 reagent ions.

219   To minimize the effect of water vapor during the ionization process inside the IMR, a water vapor

220   control system consisting of a regulated flow of a dopant (i.e., organic compound) can be injected directly

221   into the IMR (Figure 1). By replacing water with a stable concentration of the dopant, a stable ion

222   distribution is obtained across the entire range of relative humidity (RH) (further discussed in section 3.2).

223   2.4 Vacuum Interface and Analyzer

224   At the exit of the Vocus AIM reactor, product ions are sampled through a 1 mm orifice into the differentially

225   pumped vacuum interface. The efficiency with which the ions at the end of the reactor are sampled depends

226   primarily on the ratio of the sample flow which exits through the orifice relative to the flow towards the

227   vacuum pump evacuating the reaction chamber. This flow split is in turn also dependent on the reactor

228   pressure but is typically ~0.5 slpm. After entering the next stage of the interface, an RF-only quadrupole

229   ion guide efficiently focuses the analyte ions into a narrow beam, leading to the net removal of the neutral

230   molecules by a vacuum pump (Ebara PDV 500). Typical RF amplitudes of 100 V_{p-p} are sufficient to focus

231   most ions without significant ion activation for the iodide-water adduct where the iodide-water adduct is a

232   very weakly bound complex that is known to respond to transfer through vacuum interfaces relative to its

233   known thermodynamic distribution. In general, reagent ions and analyte ions that are very weakly bound

234   to the reagent ions (e.g., water cluster with a binding energy of 10 kcal/mol) (Caldwell et al., 1989) are

235   often observed to deviate from the thermodynamic distribution with RF amplitudes >50 Vp-p. This is not

236   entirely problematic, as the binding energy of these complexes is usually too weak for sensitive detection

237   even at the weakest transfer conditions. For typical analytes with moderate binding energies (e.g., iodide-

238   formic acid adducts), no significant declustering is observed at RF amplitudes <125 V_{p-p}. We find that the

239   optimal voltage gradients in the first quadrupole region are typically all 0 V between electrodes, as ions are

240   focused on the radial direction efficiently by the RF but transported axially by the gas flow. This ensures

241   that ions are transmitted with the lowest possible added energy into the next stage of the vacuum interface.

242   The rest of the differentially pumped interface is pumped by a single split flow turbo pump (Pfeiffer SF270)

243   and consists of an additional segmented quadrupole ion guide held at 10^{-2} mbar which transfers

244 energetically cooled ions into a lens stack held at 10^{-5} mbar before an orthogonal extraction in a time-of-

245 flight mass analyzer (Tofwerk Vocus CI-TOF 2R) operated at $<10^{-6}$ mbar The instrument was configured

246 to measure a mass-to-charge (m/Q) range of $1-900$ Th (12 kHz extraction frequency) with a mass resolving

247 power of 10 000 – 11 000 for the experiments described herein.

248   2.5 Flow Tube Oxidation Experiments

249 Ozonolysis/OH radical initiated oxidation of α-pinene ($C_{10}H_{16}$) experiments were performed under dry

250 conditions, at room temperature and atmospheric pressure in a flow tube reactor. The reactor consisted of

251 a ~ 6-litre Pyrex glass tube (80 mm i.d., × 120 cm length). The total flow rate of dry synthetic air (N_2/O_2

252 80:20) was set at 5.5 slpm giving an average residence time of 70 seconds. Mixing ratio of 60 -70 ppb of

253 ozone generated by an ozone generator (Fisher Scientific, SOG-1) was continuously injected into the flow

254 tube. A mixing ratio of 200 ppb α-pinene was introduced from a homemade gas cylinder (40 ppm in UHP

255 N_2). The sample was immediately sampled into the reactor at a sample flow rate of 1.8 slpm with the excess

256 flow going to exhaust.

257   2.6 Calibration

258 To measure the instrument's sensitivity, we calibrated the reactor using different compounds each selected

259 to follow general structural selectivity rules for each ion chemistry. For example, no sensitivity for xylene

260 is reported for negative ions, as negative ions like iodide do not detect xylene with any significant

261 sensitivity. To calibrate benzene cations, we used a multicomponent gas (Apel Riemer Environmental Inc)

262 containing a mixture of hydrocarbons and ketones (Table S1). An internal calibration gas system consisting

263 of two mass flow controllers (Bronkhorst, capacity 30 and 2000 sccm) and a mixing volume diluted a flow

264 of 10 sccm of the gas standard into a carrier flow of 2000 sccm of UHP nitrogen resulting in a final mixing

265 ratio for each compound present in the gas mixture of 5 ppb. For iodide anions and protonated acetone

266 dimers, a liquid calibration system (LCS v2, Tofwerk) was used to form standard concentrations of lower

267 volatile species not compatible with gas cylinders. By introducing a continuous flow of liquid with known

268 concentration into a nebulizer and aluminum evaporation chamber, the LCS provides a continuous,

269   calibrated gas-phase concentration to the instrument. The evaporation chamber of the LCS was set to a

270   temperature of 150 °C, with a UHP nitrogen flow rate of 2000 sccm thereby slightly overflowing the sample

271   inlet. For the lower volatility compounds, we cannot rule out losses in the LCS, but find that collision-

272   limited sensitivities between positive and negative ion modes agree well within experimental uncertainty.

273   Aqueous solutions with concentrations ranging from 5 to 50 µM, and liquid flow rates of 10 µL/min, were

274   used to reach target concentrations in the low ppb range for each molecule and maintain constant water

275   vapor concentrations during calibration. Ammonia concentrations were generated using a gas standard and

276   independently compared to a cavity ring-down spectroscopy gas analyzer (Picarro Model G2508) to

277   validate the sensitivity and linearity of protonated acetone dimers towards ammonia (Figure S2).

278   Instrument backgrounds and detection limits are determined by measuring UHP nitrogen at the entrance

279   of the reactor. We note that measuring the total background should include any background measurement

280   of sampling inlets, but such characterization and best practices for sampling is beyond the scope of this

281   paper and discussed in detail elsewhere (Palm et al., 2019; Riva et al., 2019). We therefore report detection

282   limits using UHP nitrogen overflowing the inlet by using the zero port which introduces zero gas just to the

283   high-pressure (atmosphere) side of the critical orifice at the entrance of the reactor. We purged the

284   instrument before and after the calibration experiment for ten minutes with UHP nitrogen to determine the

285   instrument background count rates. As reported in detail previously (Palm et al., 2019), during a background

286   measurement the reactor walls are pushed out of equilibrium by the incoming clean air. This perturbation

287   can impart a transient effect on different compounds depending on primarily volatility. For volatile and

288   extremely low volatile compounds the response to a step change in concentration (introduction of zero air)

289   is close to instantaneous (< 100 ms) due to negligible adsorption (sticking rate), for the volatile species and

290   effectively infinitely slow evaporation rates from walls for the lowest volatility compounds (irreversible

291   loss). For background determinations the most challenging group of compounds are intermediate and semi-

292   volatile compounds which readily respond to changing inlet conditions and partition back and forth between

293   the reactor walls and the reactor flow. In laboratory conditions or at ground sites where temporal changes

294   are often only slowly changing, we use dry UHP N_2 to replace the incoming sample air for 1 minute. As

295 noted in prior work, under more dynamic environments the duration and frequency of instrument

296 background measurements should be decreased and increased respectively to match the temporal changes

297 which are to be measured.

## 3. Results and discussion

3.1. Vocus AIM time response

300 Real time measurements require fast time response to report temporal trends in measured concentrations

301 accurately. For many compounds, the time response can approach that of the volumetric time response of

302 the reactor (3 ~ 30 ms), however for semi-volatile (i.e., sticky) compounds the time response is often

303 observed to be much slower than the volumetric time constant as interaction with the reactor walls results

304 in smearing of the concentration over time. The primary interaction of the analyte and the reactor walls

305 defines the response time at constant temperature, pressure, and flow. Therefore, optimizing the shape and

306 the materials of the wetted surfaces is critical to maintaining a fast response. The Vocus AIM reactors'

307 conical design notably improves the time response by ensuring that the walls get further and further from

308 the exit orifice along the length of the reactor. This shape increases the probability that vapors that have

309 interacted with the wall are pumped away instead of being ionized and transferred into the mass analyzer.

310 It also ensures that in the region of the primary expansion, the recirculation eddies do not have significant

311 space to form, allowing a faster equilibration time at the entrance of the reactor (Figure 1). To accurately

312 measure dynamic changes in concentration, particularly for low-volatility species like oxidized organics,

313 inorganic acids, and reactive species, cPTFE is chosen as the reactor wall material. Teflon® based materials

314 have on average the weakest interaction with most organic and inorganic compounds (Morris et al., 2023)

315 and are therefore a good choice for the reactor walls. cPTFE in particular is chosen as its conductivity

316 prevents surface charge-up of the reactor walls which would result in unstable or slowly equilibrating ion

317 signals. We evaluate the performance of the reactor using molecules that represent a worst-case scenario

318 i.e., have a high surface affinity and interact strongly with the walls of the reactor. In Figure 2 we compare

319 the measurement of nitric acid in the AIM reactor with iodide adduct ionization with other IMR reactors

320 (Lee et al., 2018; Palm et al., 2019) with different approaches to improve the time response, notably a very

321 short stainless steel tubular reactor, and a larger flow tube reactor with laminarizer and sheath flow operated

322 at reduced pressure. To quantitatively compare the time responses of these different reactors we measured

323 the decay time, defined as the duration for the signal to fall below 90% of its peak value after the source of

324 nitric acid is removed. While the response time of the Vocus AIM reactor is not instantaneous, it is roughly

325 a factor of 3-4 faster than previously published medium pressure reactors. The improved time response is

326 most critical for ensuring that the memory effect in the reactor is minimized, crucial for applications where

327 fast transients need to be quantified, for example in mobile laboratories, aircraft, or flow tube reactors.

328   3.2 Water Vapor Control and Suppression.

329 A major limitation of chemical ionization reactors operated at elevated pressure is that water vapor can

330 strongly impact the net reaction mechanism and reagent ion distribution resulting in sensitivities that are

331 humidity-dependent (Zhang W. et al., 2023; Zhang Y. et al., 2023) as shown in Figure S3 for the reagent

332 ion distribution. Such changes pose considerable challenges for accurate quantification of species in

333 conditions where humidity is variable. The sensitivity to a given compound will depend on whether water

334 vapor competes with it for the reagent ion, i.e., lowering the sensitivity, or whether the presence of water

335 molecule offers a loosely bound third body to stabilize the adduct by removing the excess energy after the

336 {M-(reagent ion)} collision, thereby increasing sensitivity. While post measurement correction can be

337 performed, it is labor-intensive and prone to errors as each compound has essentially a unique humidity

338 dependence. To overcome this fundamental drawback, the Vocus AIM reactor introduces a system to

339 mitigate water vapor dependencies using a dopant. The dopant effectively replaces water vapor, the

340 dominant ligand in the switching reaction involving the reagent ions and the analyte molecules. A dopant

341 could in principle be any molecule that binds (forms an adduct) with the reagent ion more strongly than the

342 reagent ion and water. In this way, the dopant can displace the water molecules that would normally be

343 attached to the reagent ions with a compound that is not variable or present in significant concentrations in

344   the sample gas. The following equations show the modified reaction mechanism in the presence of a dopant

345   (D) in the case of iodide anions.

346
$$I(H_2O)n^- + M \rightarrow IM^- + (H_2O)n \qquad (8)$$

347
$$ID^- + M \rightarrow IM^- + D \qquad (9)$$
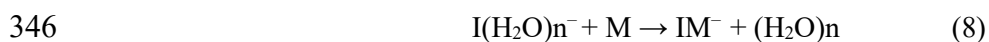
348   The modified reaction mechanism no longer significantly depends on varying water vapor conditions as

349   long as the dopant molecule is present in sufficiently high concentrations to replace most of the water

350   ligand. In the above chemical ionization mechanism for iodide anions, the challenge can be to choose a

351   suitable dopant. While the dopant must efficiently displace the water that is bound to iodide, it is also

352   desirable for the binding energy to be close to that of water. This ensures that the net chemical ionization

353   selectivity remains nearly unchanged compared to the dopant-free conditions. If a dopant with a very high

354   binding energy is selected, it will introduce a binding energy ionization threshold which will significantly

355   change the selectivity of the given ion chemistry by essentially removing all weakly bound adducts from

356   the spectra. Here we investigate three different dopants including acetonitrile, methanol, and acetone. These

357   compounds weakly interact with iodide anions and have a high vapor pressure which facilitates their easy

358   introduction into the reactor. This is typically achieved using a mass flow controller (Bronkhorst Low Delta

359   P, 30 sccm MFC) that draws from the headspace of a liquid reservoir, effectively minimizing the net dilution

360   (net sample dilution ~1%).

361   For each of the evaluated dopants, stable concentrations of formic, nitric, and acrylic acids were

362   introduced into the entrance of the reactor. The incoming air was humidified with two mass flow controllers,

363   one delivering dry nitrogen and the other passing dry nitrogen through a water bubbler held at room

364   temperature. The ratio of the two mass flow controllers was programmatically changed to simulate changes

365   in sample humidity for each dopant flow rate. Figure 3 illustrates how the systematic introduction of each

366   of these dopants at different mass flow rates influences the reactor's detection efficiency for nitric, formic,

367   and acrylic acids under changing humidity levels (0 - 100% relative humidity at 25˚C). These compounds

368   were selected as characteristic compounds for the iodide adduct system, each demonstrating a distinct

369   sensitivity dependence on humidity which follows the changes in the water-iodide cluster distribution (Lee

370   et al., 2014).

371   Under dopant-free conditions, we expect nitric acid to first sharply increase from dry conditions to

372   humid conditions followed by a plateau at water vapor partial pressures of ~0.25 mbar. This can be

373   attributed to nitric acid's high binding enthalpy with I^- and a small, (1kcal/mol), difference to the binding

374   enthalpy to $I(H_2O)^-$ that is sufficiently compensated by the kinetic stabilization from the increased number

375   of vibrational modes due to the addition of the water molecule (Lopez et al., 2016). In the case of acrylic

376   acid, the sensitivity as a function of water vapor concentration falls rapidly following the availability of

377   unhydrated iodide anions. With increasing water vapor concentrations, the weak binding energy between

378   acrylic acid is not enough to overcome the competition with water for the bare iodide ions. Formic acid is

379   between these two extremes, initially stabilized by the presence of water, but ultimately in competition with

380   water for iodide ions as the second water cluster forms reducing the sensitivity at higher absolute humidity.

381   In the doped conditions, the humidity dependencies are significantly reduced for all molecules. The

382   dopant and humidity scans demonstrate the net effect of the different dopants for each molecule as a

383   function of the total dopant flow introduced. While methanol and acetone to a certain extent shift the reagent

384   ion distribution, they are not present in high enough concentrations to fully displace the water and stabilize

385   the reagent ion distribution against changes driven by humidity changes. Acetonitrile on the other hand

386   demonstrates a significant shift in reagent ion distributions and a significant damping of the humidity

387   dependency, particularly at flows greater than ~20 sccm. With acetonitrile as the dopant, the change in

388   sensitivity across the humidity range is reduced to a deviation of <20% relative to dry conditions for all

389   model compounds, more for formic acid and nitric acid (<10 %). From the relative flattening of the humidity

390   dependence, for iodide anions (Caldwell et al., 1989) acetonitrile emerges as the most efficient dopant tested

391   reducing sensitivity variability across most analytes to a deviation that becomes negligible for ambient

392   analysis.

393   While this example focused on the dopant's presence in the reaction mechanism for iodide anions,

394   the same concept holds for any adduct forming ion including Br^- and Cl^-. For example, when generating

395   protonated ammonium ions in the presence of acetone, the formation of the $C_3H_6O–NH_4^+$ adduct with

396   acetone itself acts as a dopant and greatly suppresses the water vapor dependency, as demonstrated in Figure

397   S4. Where ammonium ions alone exhibit order of magnitude humidity dependencies when operated at

398   elevated pressure, this variability is reduced to <30% with significant acetone present as the dopant

399   (Canaval et al., 2019; Xu et al., 2022; Li et al, 2023), greatly simplifying analysis.

400   ### 3.3 Sensitivity and Limits of Detection

401   Sensitivities for a variety of compounds were evaluated for each ion chemistry to quantify the overall

402   instrument performance. Calibrations were typically done at one or two different concentration steps in the

403   range of a few ppbv. Sensitivities were normalized to the number of recorded reagent ions measured at the

404   detector, which provides a straightforward method for correcting for any absolute fluctuations in the

405   instrument's response over time and referenced to a recorded total reagent ion current of 10^6 ions/second.

406   Typical reagent ion currents measured on the Vocus AIM reactors are between $3 – 6 \times 10^6$ ions/second for

407   iodide anions and benzene cations. Results from the calibration experiments are summarized in Table 1

408   organized by reagent ion. The compounds for calibration were specifically selected based on their

409   selectivity for each reagent ion and their relative ease of producing stable concentrations. A diverse range

410   of hydrocarbons, reactive nitrogen species, organic compounds (with various volatilities), and inorganic

411   acids can be detected with high sensitivities often greater than ~10 cps/ppt/1 x 10^6 RI. The sensitivity of

412   the Vocus AIM reactor does not necessarily surpass that of previous low and medium-pressure reactors

413   (Lee et al., 2014, 2018; Ye et al., 2021; Xu et al., 2022) in an absolute sense, however, the sensitivity is in

414   the same approximate range and reaches the extremely low limit of detections (LoD) ranging from 0.1 to 5

415   ppt for most compounds. LoD measurements were performed by introducing 2 slpm of dry UHP N2 (i.e.,

416   background measurement) for 10-15 minutes. The LoD was estimated by using Tofware and calculating

417   the Allan variance (i.e., the stability of the signal over time). Finally, the LoD corresponds to 3 standard

418   deviations (sigma) of the Allen variance and is determined as a function of integration time estimation. An

419   example, using acetone dimers as reagent ions, the LoD for ammonia is about 10 ppt (1 min averaging),

420   which is 1-8 times lower than previously reported for this compound (You et al., 2014; Dong et al., 2022;

421   Schobesberger et al., 2022). Additionally, using a benzene cation as a reagent ion, the LoD for

422   monoterpenes (e.g., 0.2 ppt for α-pinene at 1 min) can even surpass conventional PTR techniques, including

423   the Vocus PTR (i.e., 4 ppt for α-pinene at 1 min; Krechmer et al., 2018) and similar to the FUSION PTR

424   (i.e., 0.1 pptv for 1 minute;).

425   The absolute sensitivity of the instrument depends fundamentally on the reaction time and collision

426   frequency (pressure) as well as the absolute number of generated reagent ions introduced into the reactor.

427   Figure 4a shows the dependence of the measured sensitivity of levoglucosan on the reactor pressure. By

428   increasing the pressure from 35 to 75 mbar the sensitivity of the instrument can be increased by a factor of

429   ~ 4 which is consistent with the increase expected based on reaction time and collision frequency. Operating

430   at higher pressures can be beneficial in pristine or highly diluted environments, where the concentrations

431   of target compounds can reside in the sub-parts-per-trillion (sub-ppt) range. A nominal operation pressure

432   of 50 mbar provides a good balance between sensitivity and linear range which under typical conditions

433   extends to ~100-200 ppbv depending on the analyte (Figure 4b). This allows the standard conditions (which

434   are a compromise between sensitivity and linear range) of the Vocus AIM reactor to operate equally well

435   in pristine and polluted environments with the same configuration. In highly polluted environments where

436   the total detectable mass concentrations greatly exceed the linear range of the instrument, reagent ion

437   normalization can compensate for up to 50% of reagent ion depletion before normalization errors begin to

438   accumulate. In such conditions, the incoming sample flow would need to be diluted, to maintain

439   concentrations within the normalization range.

440   Finally, taking advantage of the improved time response and the possibility of operating more than

441   one VUV lamp on the Vocus AIM reactor (Figure 1), a fast switch between different ion chemistries at up

442   to 2 Hz is now possible as shown in Figure S5. This valuable feature allows the Vocus AIM reactor to

443   extend the variety of compounds detected by one instrument within a single polarity, as the mass analyzer

444   used in this study had polarity switching timescales of 5-10 minutes.

445

446   3.4 Vocus AIM Performance for Atmospheric Applications

447   To evaluate the bulk detection capabilities of Vocus AIM we measured oxidation products from the OH/O_3

448   initiated oxidation of α-pinene using a steady-state flow tube setup. This reaction mechanism was chosen

449   because it is a well-studied system resulting in a suite of oxidation products spanning a wide range of

450   functionalities. Additionally, it generates molecules with a wide range of molecular masses, from lightly

451   oxidized monomers to heavily oxidized dimers. In total, four AIM reagent ion chemistries, namely NH_4^+,

452   Cl^-, I^- and NO_3^- were used to investigate their relative detection efficiency (selectivity) towards produced

453   OVOCs. AIM offers an ideal method for evaluating ion chemistries as it ensures uniformity in the

454   introduction of all reagent ions and utilizes the same analytical instrument for comparison. This approach

455   effectively eliminates the instrument-to-instrument variability, thus providing a highly direct and unbiased

456   comparison of ion chemistry and detection efficacy for a variety of mixed organic compounds.

457   RO_2 radicals generated from the combined ozonolysis and OH radical reaction of α-pinene can

458   further react yielding mixed oxidation products during the reaction time in the flow tube. Among the

459   different RO_2 radicals formed, $C_{10}H_{15}O_{>3}$ and $C_{10}H_{17}O_{>2}$ were detected by the different reagent ions used.

460   While the mass spectra are generally similar between the different reagent ion chemistries, there are some

461   notable differences in the detection efficiencies. NO_3^- ion-based chemistry is by far the most selective of

462   the reagent ions tested. A smaller group of compounds was detected, with a particular inclination towards

463   the most heavily oxidized monomers and gas-phase dimer species. The variable selectivity of the different

464   ion chemistries is demonstrated in Figure 5, organized by the increase of reagent ion selectivity. NH_4^+ and

465   Cl^- are the least selective ions evaluated, highlighted by the large ion signal intensity of compounds m/Q <

466   100 Th (least oxidized) and the largest number of absolute compounds detected. While the sensitivity

467   towards less oxidized compounds is limited to the less selective reagent ions (i.e., NH_4^+ and Cl^-), more

468   selective reagent ions excel at detecting the lower concentration of more oxidized compounds. The

469   selectivity of the reagent ion plays a pivotal role in limiting the backgrounds and potential isobaric

470   interferences that might hamper the detection of the compounds of interest. With the AIM reactor and the

471   right selection of reagent ion, even the highest oxidized RO_2 radicals (e.g., $C_{10}H_{17}O_7$ and $C_{10}H_{15}O_8$), and

472   dimeric products (e.g., $C_{19}H_{28,30}O_x$ $C_{20}H_{30,32}O_x$) can be identified under relevant atmospheric conditions,

473   highlighting the very high sensitivity and versatility of the Vocus AIM reactor.

474   To demonstrate the bulk detection properties of the different reagent ion chemistries more clearly,

475   we categorized each compound according to its estimated volatility. Due to the lack of authentic standards

476   measuring the vapor pressure of oxygenated organic molecules (OOMs) remains an analytical challenge.

477   To overcome this problem, model calculations have been developed to estimate the vapor pressure using,

478   for example, structure-based estimations and formula-based estimations. The volatility basis set (VBS)

479   framework has been established by Donahue et al. (2011) and is widely used in atmospheric chemistry to

480   estimate the volatility of products measured by mass spectrometry techniques. The VBS parameterization

481   is useful for classifying the wide range of OOMs into multiple volatility groups, including extremely low

482   volatility organic compounds (ELVOC) and low volatility organic compounds (LVOC) based on their

483   effective saturation concentration (C*) in the unit of μg m^{-3}. In this work, we apply the VBS

484   parameterization optimized by Li et al. (2016),

$$log_{10}C^*(298K) = \left(n_C^0 - n_C\right)b_C - n_O b_O - 2\frac{n_C n_O}{(n_C + n_O)}b_{CO} - n_N b_N - n_S b_S \tag{10}$$

485

486   where n_C, n_O, n_N, and n_S are the number of carbon, oxygen, nitrogen, and sulfur atoms of the specific

487   molecule, separately; n^0_C is the reference carbon number; b_C, b_O, b_N, and b_S are the contribution of each

488   atom to $log_{10}C^*$, respectively; b_{CO} is the carbon-oxygen nonideality. The b coefficient values can be found

489   in Li et al. (2016). In this study, all oxidation products generated from the OH/O_3 initiated oxidation were

490   grouped into six volatility regimes; ultralow-volatility (ULVOCs, C* < $10^{-8.5}$ μg m^{-3}), extremely low

491   volatility (ELVOCs, $10^{-8.5}$ < C* < $10^{-4.5}$ μg m^{-3}), low-volatility (LVOCs, $10^{-4.5}$ < C* < $10^{-0.5}$ μg m^{-3}), semi-

492   volatile (SVOCs, $10^{-0.5}$ < C* < $10^{2.5}$ μg m^{-3}), intermediate-volatility organic compounds (IVOC, $10^{2.5}$ < C*

493   < $10^{6.5}$ μg m^{-3}), and VOC ($10^{6.5}$ < C* μg m^{-3}) based on VBS.

494   Figure 6 illustrates the measured range of oxidation products generated by the hydroxyl radical and

495   ozone reaction with α-pinene. These products were analyzed using one mass spectrometer with AIM reactor

496   setup employing various ionization chemistries. Therefore, unlike other studies (Riva et al., 2019, Li et al.,

497   2023) this study utilizes a single instrument, thereby reducing uncertainties associated with the calibration

498   and settings of different instruments as well as the conditions during sample collection. The total signal in

499   each volatility bin represents the sum of the signal intensity of OOMs within the volatility range. Organic

500   compounds with C^* of $< 10^{-1}$ μg m^{-3} made up the largest signal contributions for the Vocus AIM using

501   NO_3^--ion based chemistry (Table S2). This observation is consistent with the conventional atmospheric

502   pressure using NO_3^- as the reagent ion and indicates that the design of the Vocus AIM reactor allows the

503   detection of ELVOC and ULVOC (Riva et al., 2019; Zhang W. et al., 2023; Zhang Y. et al., 2023). This is

504   a substantial improvement for the atmospheric science community as measurement of such species is solely

505   possible with the use of atmospheric pressure interfaces which can be associated with sensitivity

506   fluctuations (e.g., RH effect). As demonstrated previously (Riva et al., 2019), I^--ion based chemistry detects

507   oxygenated compounds with C^* ranging from 10^{-5} to 10^5 μg m^{-3} which corresponds to OOMs and start

508   being less sensitive to oxygenated compounds having fewer oxygen atoms and are included in the IVOC

509   fraction. While Cl^- and NH_4^+ can also measure OOM with C^* as low as 10^{-5} μg m^{-3} the weak selectivity of

510   these ion-based chemistries allows them to measure a wider range of compounds (i.e., IVOCs and VOCs).

511   IVOCs and VOCs generally include less oxygenated VOCs with shorter carbon skeletons and comprise the

512   main fraction of organics formed from the oxidation of pinene (Isaacman-VanWertz et al., 2018). We stress

513   here that while it was not possible to detect ULVOC and ELVOC using I^-, Cl^-, NH_4^+-ion based chemistries

514   it is purely a selectivity limitation of the more general reagent ions not of absolute sensitivity as all the

515   tested reagent ions have similar overall absolute sensitivities. Nitrate reagent ions benefit from the high

516   selectivity, which also manifests in a lower background signal therefore enabling nitrate anion chemistry to

517   detect ULVOC and ELVOC. With the significantly lower background concentrations of nitrate ions, the

518   detection of compounds at extremely low concentrations (as low as 10-100 ppqv) becomes possible.

519   Differences in the contribution of these compound groups (i.e., relative signal contribution to total

520   OOMs) with previous work could be due to different sensitivities of the instruments towards organic

521   compounds with varying oxidation extents (Riva et al., 2019). In addition, experimental conditions (e.g.,

522   RH, temperature, precursor concentration) and setup (flow tube reactor, atmospheric simulation chambers)

523   can greatly impact the distribution of OOMs retrieved by MS techniques. By carefully selecting the type of

524   reagent ion, the combined volatility distribution can cover from VOCs to OOMs, with varying O:C ratios

525   and volatility ranges (Figure 6) all within a single instrument. The Vocus AIM can therefore provide a more

526   complete picture of the volatility distribution of gaseous organic and inorganic compounds found in the

527   atmosphere.

Conclusions

529   The primary goal of this work was to evaluate the performance of the newly designed Vocus AIM reactor

530   to determine the time response, sensitivity, and selectivity using multiple reagent ions. Of specific

531   importance, we introduced and demonstrated the utility of a dopant-based water vapor suppression system

532   which improves data quality and reduces the number of corrections required during analysis. By comparing

533   detection efficiency for different compounds, we demonstrated that the Vocus AIM captures nearly the

534   entire range of OVOC, spanning from VOC to ULVOC by using different types of reagent ions. Through

535   the optimization of reactor geometry and materials, the time response of the Vocus AIM reactor is greatly

536   improved even for sticky and reactive compounds. The high sensitivity achieves sub-ppt detection limits

537   for a range of VOCs and VICs. The innovative design of the new reactor substantially eliminated this

538   humidity sensitivity, facilitating more straightforward measurements of samples with water vapor and

539   simplifying data interpretation. This improvement is crucial for robust and reliable analysis across a

540   spectrum of environmental samples. As a result, the Vocus AIM reactor represents a highly versatile

541   platform able to measure the wide variety of VOCs and VICs in the atmosphere using a single instrument.

542

Conflicts of interest

All (co-)authors, except S.P. and J.A.T. work for Tofwerk AG, which is commercializing the Vocus-AIM mass spectrometer.

Author Contributions

M.R., V.P., F.L., conceive the study. M.R., V.P., C.F., P.B., S.P., S.J., and F.L. collected and analyzed the data. P.S., U.R., and F.L. conceived the design of the Vocus AIM reactor. M.R., V.P., F.L. wrote the manuscript. All authors discussed the results and commented on the paper.

References

Berndt, T., Richters, S., Kaethner, R., Voigtlander, J., Stratmann, F., Sipila, M., Kulmala, M., and Herrmann, H.: Gas-Phase Ozonolysis of Cycloalkenes: Formation of Highly Oxidized RO_2 Radicals and Their Reactions with NO, NO_2, SO_2, and Other RO_2 Radicals, J. Phys. Chem. A, 119, 10336-10348, 10.1021/acs.jpca.5b07295, 2015.

Berndt, T., Herrmann, H., and Kurten, T.: Direct Probing of Criegee Intermediates from Gas-Phase Ozonolysis Using Chemical Ionization Mass Spectrometry, J. Am. Chem. Soc., 139, 13387-13392, 10.1021/jacs.7b05849, 2017.

Berndt, T., Mentler, B., Scholz, W., Fischer, L., Herrmann, H., Kulmala, M., and Hansel, A.: Accretion Product Formation from Ozonolysis and OH Radical Reaction of alpha-Pinene: Mechanistic Insight and the Influence of Isoprene and Ethylene, Environ. Sci. Technol., 52, 11069-11077, 10.1021/acs.est.8b02210, 2018.

Bertram, T. H., Kimmel, J. R., Crisp, T. A., Ryder, O. S., Yatavelli, R. L. N., Thornton, J. A., Cubison, M. J., Gonin, M. and Worsnop, D. R.: A field-deployable, chemical ionization time-of-flight mass spectrometer, Atmos. Meas. Tech., 4(7), 1471–1479, doi:10.5194/amt-4-1471-2011, 2011.

Bianchi, F., Kurten, T., Riva, M., Mohr, C., Rissanen, M. P., Roldin, P., Berndt, T., Crounse, J. D., Wennberg, P. O., Mentel, T. F., Wildt, J., Junninen, H., Jokinen, T., Kulmala, M., Worsnop, D. R., Thornton, J. A., Donahue, N., Kjaergaard, H. G., and Ehn, M.: Highly Oxygenated Organic Molecules (HOM) from Gas-Phase Autoxidation Involving Peroxy Radicals: A Key Contributor to Atmospheric Aerosol, Chem. Rev., 119, 3472-3509, 10.1021/acs.chemrev.8b00395, 2019.

Breitenlechner, M., Fischer, L., Hainer, M., Heinritzi, M., Curtius, J., and Hansel, A.: PTR3: An Instrument for Studying the Lifecycle of Reactive Organic Carbon in the Atmosphere, Anal. Chem., 89, 5824-5831, 10.1021/acs.analchem.6b05110, 2017.

Breitenlechner, M., Novak, G. A., Neuman, J. A., Rollins, A. W., and Veres, P. R.: A versatile vacuum ultraviolet ion source for reduced pressure bipolar chemical ionization mass spectrometry, Atmos. Meas. Tech., 15, 1159–1169, https://doi.org/10.5194/amt-15-1159-2022, 2022.

Bruderer, T., Gaisl, T., Gaugg, M.T., Nowak, N., Streckenbach, B., Müller, S., Moeller, A., Kohler, M., and Zenobi, R.: On-Line Analysis of Exhaled Breath, Chem. Rev., 119, 19, 10803–10828, 10.1021/acs.chemrev.9b00005, 2019.

Caldwell, G. W., Masucci, J. A., and Ikonomou, M. G.: Negative ion chemical ionization mass spectrometry—binding of molecules to bromide and iodide anions, Organic Mass Spectrometry, 24, 8–14, 10.1002/oms.1210240103, 1989.

Canaval, E., Hyttinen, N., Schmidbauer, B., Fischer, L., and Hansel, A.: NH_4^+ Association and Proton Transfer Reactions With a Series of Organic Molecules, Front. Chem., 7, 10.3389/fchem.2019.00191, 2019.

Crounse, J. D., Nielsen, L. B., Jørgensen, S., Kjaergaard, H. G., and Wennberg, P. O.: Autoxidation of Organic Compounds in the Atmosphere, J. Phys. Chem. Lett., 4, 3513-3520, 10.1021/jz4019207, 2013.

Donahue, N. M., Epstein, S. A., Pandis, S. N., and Robinson, A. L.: A two-dimensional volatility basis set: 1. organic-aerosol mixing thermodynamics, Atmos. Chem. Phys., 11, 3303-3318, 10.5194/acp-11-3303-2011, 2011.

Dong, F., Li, H., Liu, B., Liu, R., and Hou K.: Protonated acetone ion chemical ionization time-of-flight mass spectrometry for real-time measurement of atmospheric ammonia, J. Environ Sci., 14, 66-74, 10.1016/j.jes.2021.07.023, 2022.

Ehn, M., Thornton, J. A., Kleist, E., Sipila, M., Junninen, H., Pullinen, I., Springer, M., Rubach, F., Tillmann, R., Lee, B., Lopez-Hilfiker, F., Andres, S., Acir, I. H., Rissanen, M., Jokinen, T., Schobesberger, S., Kangasluoma, J., Kontkanen, J., Nieminen, T., Kurten, T., Nielsen, L. B., Jorgensen, S., Kjaergaard, H. G., Canagaratna, M., Maso, M. D., Berndt, T., Petaja, T., Wahner, A., Kerminen, V. M., Kulmala, M., Worsnop, D. R., Wildt, J., and Mentel, T. F.: A large source of low-volatility secondary organic aerosol, Nature, 506, 476-479, 10.1038/nature13032, 2014.

Eisele, F.L., Tanner, D.J., Measurement of the gas phase concentration of H2SO4 and methane sulfonic acid and estimates of H2SO4 production and loss in the atmosphere, J. Geophys. Res. Atmo., 98, 9001-9010, 10.1029/93JD00031, 1993.

Hallquist, M., Wenger, J. C., Baltensperger, U., Rudich, Y., Simpson, D., Claeys, M., Dommen, J., Donahue, N. M., George, C., Goldstein, A. H., Hamilton, J. F., Herrmann, H., Hoffmann, T., Iinuma, Y., Jang, M., Jenkin, M. E., Jimenez, J. L., Kiendler-Scharr, A., Maenhaut, W., McFiggans, G., Mentel, T. F., Monod, A., Prévôt, A. S. H., Seinfeld, J. H., Surratt, J. D., Szmigielski, R., and Wildt, J.: The formation, properties and impact of secondary organic aerosol: current and emerging issues, Atmos. Chem. Phys., 9, 5155-5236, 10.5194/acp-9-5155-2009, 2009.

Hansel, A., Scholz, W., Mentler, B., Fischer, L., and Berndt, T.: Detection of RO2 radicals and other products from cyclohexene ozonolysis with NH_4^+ and acetate chemical ionization mass spectrometry, Atmo. Environ., 186, 248-255, 10.1016/j.atmosenv.2018.04.023, 2018.

Isaacman-VanWertz, G. and Aumont, B.: Impact of organic molecular structure on the estimation of atmospherically relevant physicochemical parameters, Atmos. Chem. Phys., 21, 6541-6563, 10.5194/acp-21-6541-2021, 2021.

Ji, Y., Huey, L. G., Tanner, D. J., Lee, Y. R., Veres, P. R., Neuman, J. A., Wang, Y., and Wang, X.: A vacuum ultraviolet ion source (VUV-IS) for iodide–chemical ionization mass spectrometry: a substitute for radioactive ion sources, Atmos. Meas. Tech., 13, 3683–3696, 10.5194/amt-13-3683-2020, 2020.

Krechmer, J., Lopez-Hilfiker, F., Koss, A., Hutterli, M., Stoermer, C., Deming, B., Kimmel, J., Warneke, C., Holzinger, R., Jayne, J. T., Worsnop, D. R., Fuhrer, K., Gonin, M. and de Gouw, J. A.: Evaluation of a New Reagent-Ion Source and Focusing Ion-Molecule Reactor for use in Proton-Transfer-Reaction Mass Spectrometry, Anal. Chem., 10.1021/acs.analchem.8b02641, 2018.

Lavi, A., Vermeuel, M. P., Novak, G. A., and Bertram, T. H.: The sensitivity of benzene cluster cation chemical ionization mass spectrometry to select biogenic terpenes, Atmos. Meas. Tech., 11, 3251–3262, https://doi.org/10.5194/amt-11-3251-2018, 2018.

Lee, B. H., Lopez-Hilfiker, F. D., Mohr, C., Kurten, T., Worsnop, D. R., and Thornton, J. A.: An iodide-adduct high-resolution time-of-flight chemical-ionization mass spectrometer: application to atmospheric inorganic and organic compounds, Environ. Sci. Technol., 48, 6309-6317, 10.1021/es500362a, 2014.

Lee, B. H., Lopez-Hilfiker, F. D., Veres, P.R., McDuffie, E.E., Fibiger, D.L., Sparks, T.M., Ebben, C.J., Green, J.R., Schroder, J.C., Campuzano-Jost, P., Iyer, S., D'Ambro, E.A., Schobesberger, S., Brown, S.S., Wooldridge, P.J., Cohen, R.C., Fiddler, M.N., Bililign, S., Jimenez, J.L., Kurtén, T., Weinheimer, A.J., Jaegle, L., and Thornton, J. A.: Flight Deployment of a High-Resolution Time-of-Flight Chemical Ionization Mass Spectrometer: Observations of Reactive Halogen and Nitrogen Oxide Species, J. Geophys Res. Atmos, 123, 7670-7686, 10.1029/2017JD028082, 2018.

Li, Y., Pöschl, U., and Shiraiwa, M.: Molecular corridors and parameterizations of volatility in the chemical evolution of organic aerosols, Atmos. Chem. Phys., 16, 3327-3344, 10.5194/acp-16-3327-2016, 2016.

Li, D., Wang, D., Caudillo, L., Scholz, W., Wang, M., Tomaz, S., Marie, G., Surdu, M., Eccli, E., Gong, X., Gonzalez-Carracedo, L., Granzin, M., Pfeifer, J., Rörup, B., Schulze, B., Rantala, P., Perrier, S., Hansel, A., Curtius, J., Kirkby, J., Donahue, N. M., George, C., El-Haddad, I., and Riva, M.: Ammonium CI-Orbitrap: a tool for characterizing the reactivity of oxygenated organic molecules, Atmos. Meas. Tech. Discuss. [preprint], https://doi.org/10.5194/amt-2023-149, in review, 2023.

Lopez-Hilfiker, F. D., Iyer, S., Mohr, C., Lee, B. H., D'Ambro, E. L., Kurtén, T. and Thornton, J. A.: Constraining the sensitivity of iodide adduct chemical ionization mass spectrometry to multifunctional organic molecules using the collision limit and thermodynamic stability of iodide ion adducts, Atmos. Meas. Tech., 9(4), 1505–1512, doi:10.5194/amt-9-1505-2016, 2016.

Mazzucotelli, M., Farneti, B., Khomenko, I., Gonzalez-Estanol, K., Pedrotti, M., Fragasso, M., Capozzi, V., and Biasioli, F.; Green Analytical Chemistry, 3, 10.1016/j.greeac.2022.100041, 2022.

Morris, M. A., Pagonis, D., Day, D. A., de Gouw, J. A., Ziemann, P. J., and Jimenez, J. L.: Absorption of VOCs by polymer tubing: implications for indoor air and use as a simple gas-phase volatility separation technique, EGUsphere [preprint], https://doi.org/10.5194/egusphere-2023-1241, 2023.

Palm, B.P., Liu, X., Jimenez, X.L., and Thornton, J. A.: Performance of a new coaxial ion–molecule reaction region for low-pressure chemical ionization mass spectrometry with reduced instrument wall interactions, Atmos. Meas. Tech., 12, 5829–5844, doi.org/10.5194/amt-12-5829-2019, 2019

Pfeifer, J., Simon, M., Heinritzi, M., Piel, F., Weitz, L., Wang, D., Granzin, M., Müller, T., Bräkling, S., Kirkby, J., Curtius, J., and Kürten, A.: Measurement of ammonia, amines and iodine compounds using protonated water cluster chemical ionization mass spectrometry, Atmos. Meas. Tech., 13, 2501–2522, https://doi.org/10.5194/amt-13-2501-2020, 2020.

Reinecke, T., Leiminger, M., Jordan, A., Wisthaler, A., and Müller, M.: Ultrahigh Sensitivity PTR-MS Instrument with a Well-Defined Ion Chemistry, Anal. Chem., 95, 11879–11884, https://doi.org/10.1021/acs.analchem.3c02669, 2023.

Rissanen, M. P., Mikkilä, J., Iyer, S., and Hakala, J.: Multi-scheme chemical ionization inlet (MION) for fast switching of reagent ion chemistry in atmospheric pressure chemical ionization mass spectrometry (CIMS) applications, Atmos. Meas. Tech., 12, 6635-6646, 10.5194/amt-12-6635-2019, 2019.

Riva, M., Rantala, P., Krechmer, J. E., Peräkylä, O., Zhang, Y., Heikkinen, L., Garmash, O., Yan, C., Kulmala, M., Worsnop, D., and Ehn, M.: Evaluating the performance of five different chemical ionization techniques for detecting gaseous oxygenated organic species, Atmos. Meas. Tech., 12, 2403-2421, 10.5194/amt-12-2403-2019, 2019.

Schobesberger, S., D'Ambro, E. L., Vettikkat, L., Lee, B. H., Peng, Q., Bell, D. M., Shilling, J. E., Shrivastava, M., Pekour, M., Fast, J., and Thornton, J. A.: Airborne flux measurements of ammonia over the southern Great Plains using chemical ionization mass spectrometry, Atmos. Meas. Tech., 16, 247–271, https://doi.org/10.5194/amt-16-247-2023, 2023.

Tang, J., Schurgers, G., and Rinnan, R.; Process Understanding of Soil BVOC Fluxes in Natural Ecosystems: A Review, Rev. Geophys., 57, 966-986, 10.1029/2018RG000634, 2019.

Vasquez, K. T., Allen, H. M., Crounse, J. D., Praske, E., Xu, L., Noelscher, A. C., and Wennberg, P. O.: Low-pressure gas chromatography with chemical ionization mass spectrometry for quantification of

679   multifunctional organic compounds in the atmosphere, Atmos. Meas. Tech., 11, 6815–6832,
680   https://doi.org/10.5194/amt-11-6815-2018, 2018.

681 Xu, L., Coggon, M. M., Stockwell, C. E., Gilman, J. B., Robinson, M. A., Breitenlechner, M., Lamplugh,
682   A., Crounse, J. D., Wennberg, P. O., Neuman, J. A., Novak, G. A., Veres, P. R., Brown, S. S., and
683   Warneke, C.: Chemical ionization mass spectrometry utilizing ammonium ions (NH4+ CIMS) for
684   measurements of organic compounds in the atmosphere, Atmos. Meas. Tech., 15, 7353–7373,
685   https://doi.org/10.5194/amt-15-7353-2022, 2022.

686 Ye, C., Yuan, B., Lin, Y., Wang, Z., Hu, W., Li, T., Chen, W., Wu, C., Wang, C., Huang, S., Qi, J., Wang,
687   B., Wang, C., Song, W., Wang, X., Zheng, E., Krechmer, J.E., Ye, P., Zhang, Z., Wang, X., Worsnop,
688   D.R., and Shao, M.,: Chemical characterization of oxygenated organic compounds in the gas phase and
689   particle phase using iodide CIMS with FIGAERO in urban air, Atmos. Chem. Phys., 21, 8455–8478,
690   https://doi.org/10.5194/acp-21-8455-2021, 2021.

691 Yuan, B., Koss, A. R., Warneke, C., Coggon, M., Sekimoto, K., and de Gouw, J. A.: Proton-Transfer-
692   Reaction Mass Spectrometry: Applications in Atmospheric Sciences, Chem. Rev., 117, 13187-13229,
693   10.1021/acs.chemrev.7b00325, 2017.

694 You, Y., Kanawade, V. P., de Gouw, J. A., Guenther, A. B., Madronich, S., Sierra-Hernández, M. R.,
695   Lawler, M., Smith, J. N., Takahama, S., Ruggeri, G., Koss, A., Olson, K., Baumann, K., Weber, R. J.,
696   Nenes, A., Guo, H., Edgerton, E. S., Porcelli, L., Brune, W. H., Goldstein, A. H., and Lee, S. H.:
697   Atmospheric amines and ammonia measured with a chemical ionization mass spectrometer (CIMS),
698   Atmos. Chem. Phys., 14, 12181-12194, 10.5194/acp-14-12181-2014, 2014.

699 Zhang, W., Xu, L., Zhang, H.: Recent advances in mass spectrometry techniques for atmospheric chemistry
700   research on molecular-level, Mass Spectrom. Rev., 21857, 10.1002/mas.21857, 2023.

701 Zhang, Y., Liu, R., Yang, D., Guo, Y., Li, M., and Hou, K.: Chemical ionization mass spectrometry:
702   Developments and applications for on-line characterization of atmospheric aerosols and trace gases,
703   Trends Anal. Chem., 168, 10.1016/j.trac.2023.117353, 2023.

704

705 **Table 1.** Sensitivities (cps pptv^{-1}) normalized by 10^6 detected reagent ions for different ion
706 chemistry used with the Vocus AIM reactor.
707

| Compounds	Reagent Ion	Sensitivity (cps/ppt/ 10^6 ions/s)	LoD (1-min)
toluene	Benzene (+)	7.8	0.4
m-xylene	Benzene (+)	7.6	0.2
1,2,4-trimethyl benzene	Benzene (+)	7.5	0.2
α-pinene	Benzene (+)	6.8	1.4
methyl ethyl ketone	Acetone-Ammonia (+)	5.0	4.8
ammonia	Acetone dimer (+)	1.5	1
methyl amine	Acetone dimer (+)	1.2	10
ethyl amine	Acetone dimer (+)	1.6	1
dimethyl amine	Acetone dimer (+)	2.2	1
diethyl amine	Acetone dimer (+)	2.6	1
trimethyl amine	Acetone dimer (+)	2.5	4
triethyl amine	Acetone dimer (+)	5.0	2
formic acid	Iodide (–)	2.0	0.8
levoglucosan	Iodide (–)	6.0	0.1
chlorine	Iodide (–)	5.5	3
nitric acid	Iodide (–)	4.3	5
fluoric acid	Iodide (–)	3	10
iodine	Bromide (–)	3	2

708

709

710
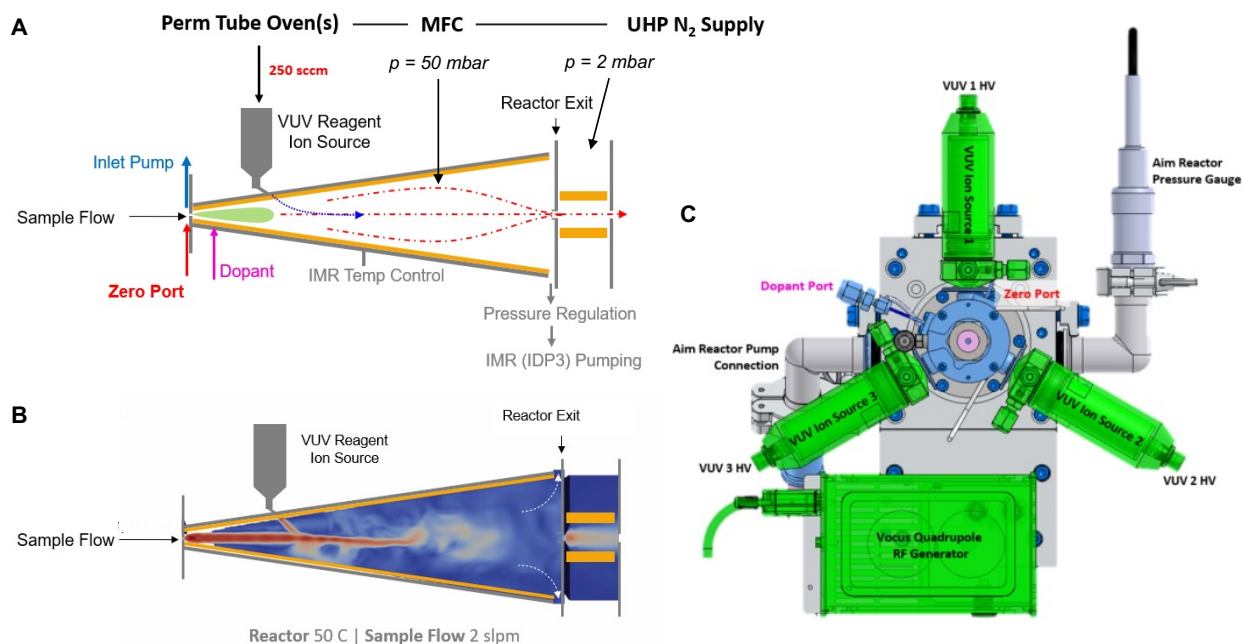
Figure 1. (A) Diagram of the Vocus AIM reactor showing the conical design and relative locations of the sample and reagent ion addition. (B) Cross-sectional view of modeled flow velocities in the AIM-IMR, showing optimized intersection of the reagent ion and sample stream flows, and limited contact of the sample gas with surfaces. Dopant flow was not considered for the CAD calculation. (C) Key components of the Vocus AIM reactor.
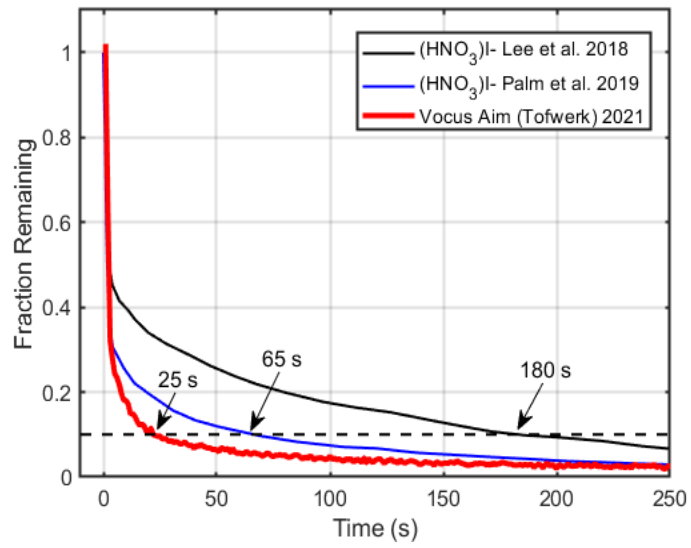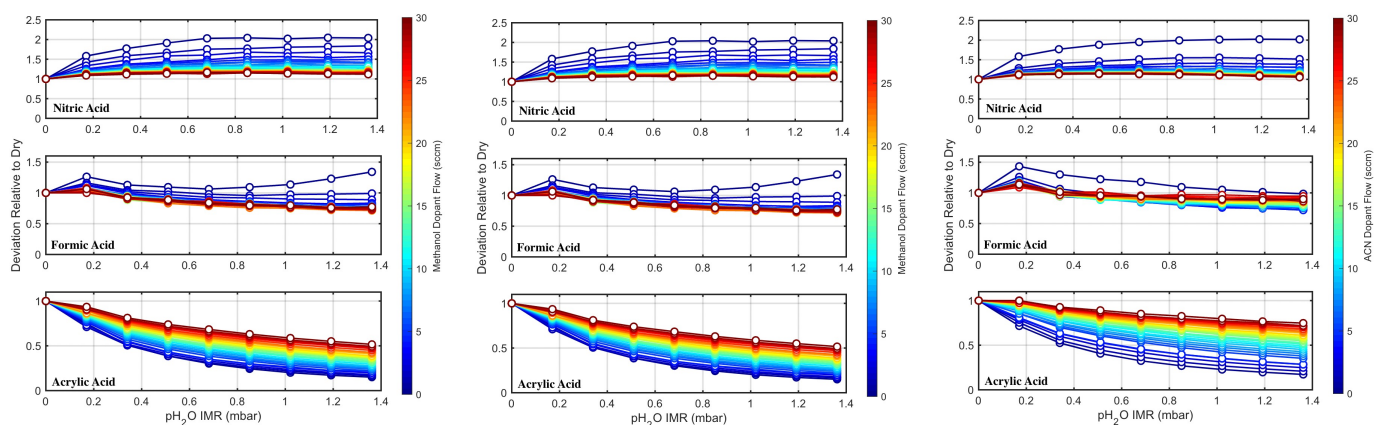
717

718 **Figure 2.** Time response to nitric acid of the Vocus AIM IMR compared to the previous IMR designs

719 found in the literature.

720

Figure 3. Impact of the relative humidity on the sensitivity of nitric acid, formic acid, and acrylic acid as a function of different dopant concentrations (dopants: acetone, methanol, and acetonitrile). The x-axis displays the partial pressure of water, corresponding to higher humidity levels within the reactor (0-100% humidity). The color gradient indicates the increasing flow of specific dopants.

725

726
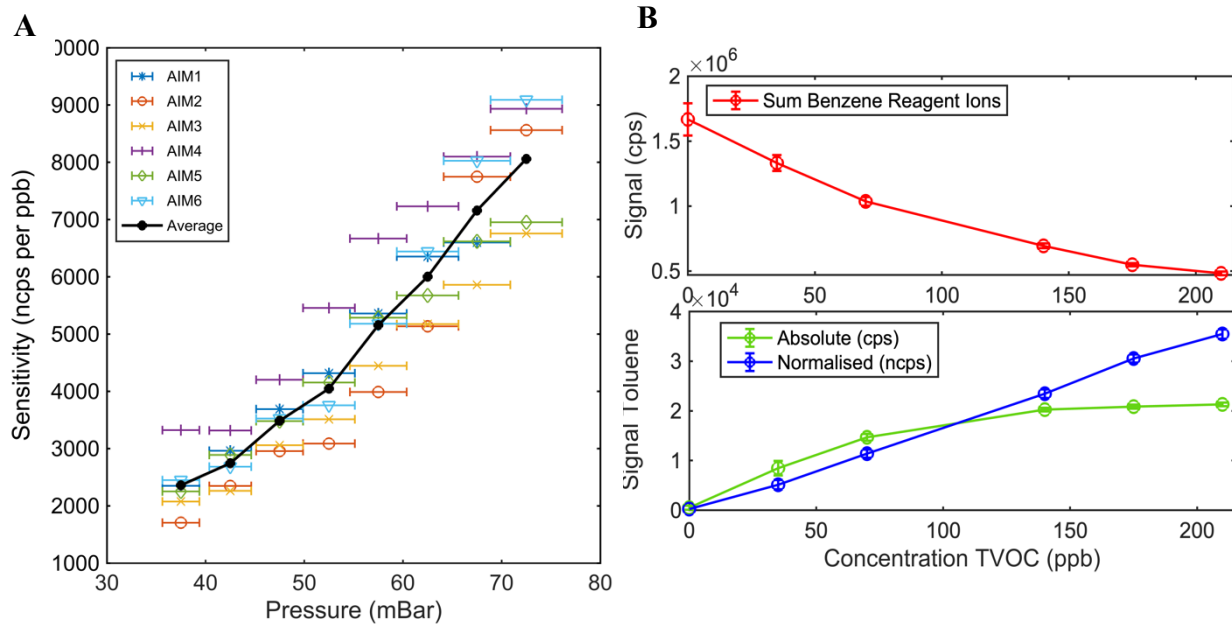
735

736 **Figure 4**. (A) presents the sensitivity dependance on the IMR pressure. The solid line represents the average

737 sensitivity from six distinct Vocus AIM instruments, each normalized to one million reagent ions.

738 Individual sensitivity measurements for each reactor are depicted as unique symbols. The error bars provide

739 an estimate of the pressure gauge measurement uncertainty within 5 % of error. (B) shows the evolution of

740 the sum of the reagent ions for Benzene cation chemistry and lower panel the ion signal intensity of toluene

741 with and without normalization to reagent ions under a wide range of concentrations.

742

743
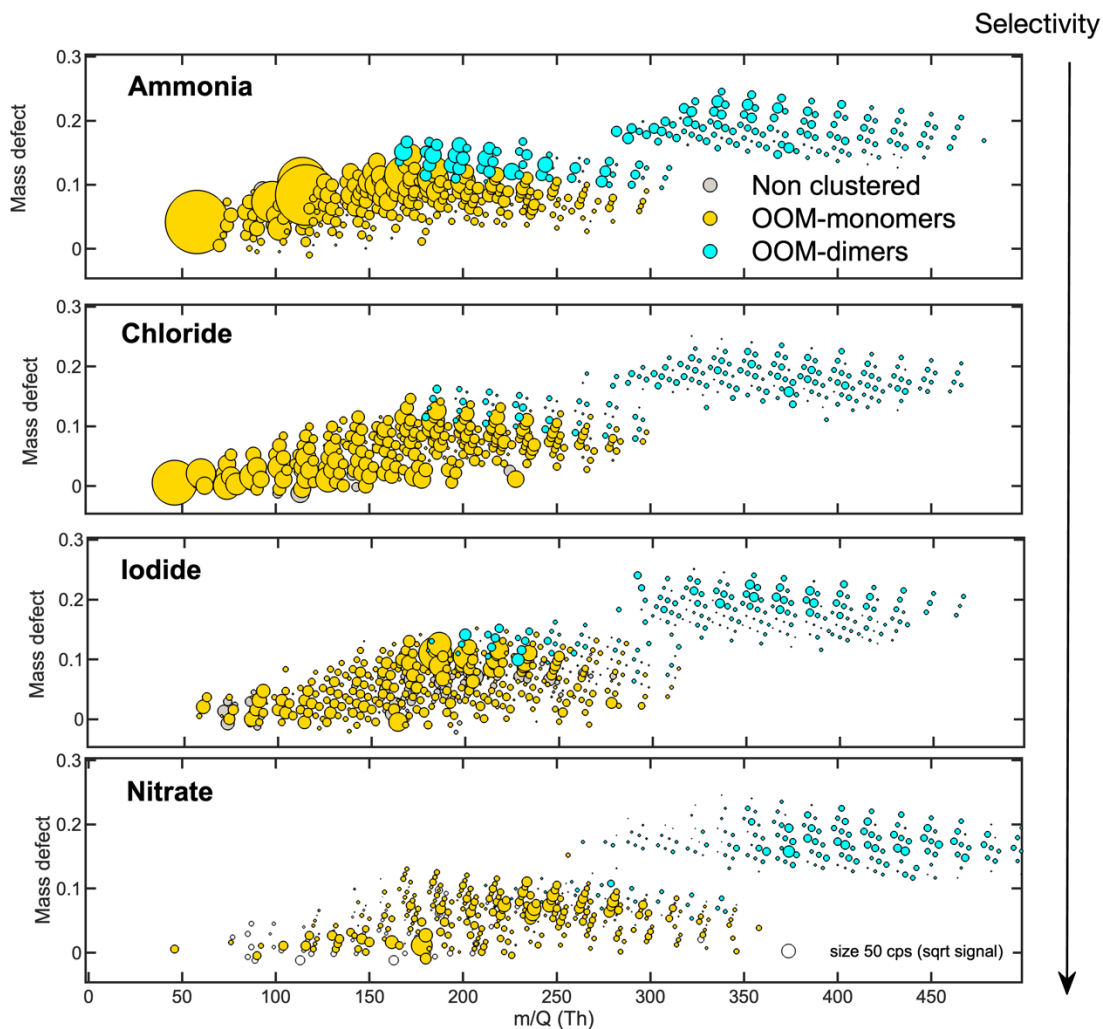
Figure 5. Mass defect plots of organic compounds measured by the Vocus AIM reactor using Ammonia, Chloride, Iodide, and Nitrate ion chemistries generated via the O_3/OH initiated oxidation of α-pinene. The x-axis represents the mass-to-charge ratio of the neutral analyte, the y-axis represents the corresponding mass defect, which is the difference between their exact mass and nominal mass, and the size of the circle represents the square root of the signal intensity measured for each ion.
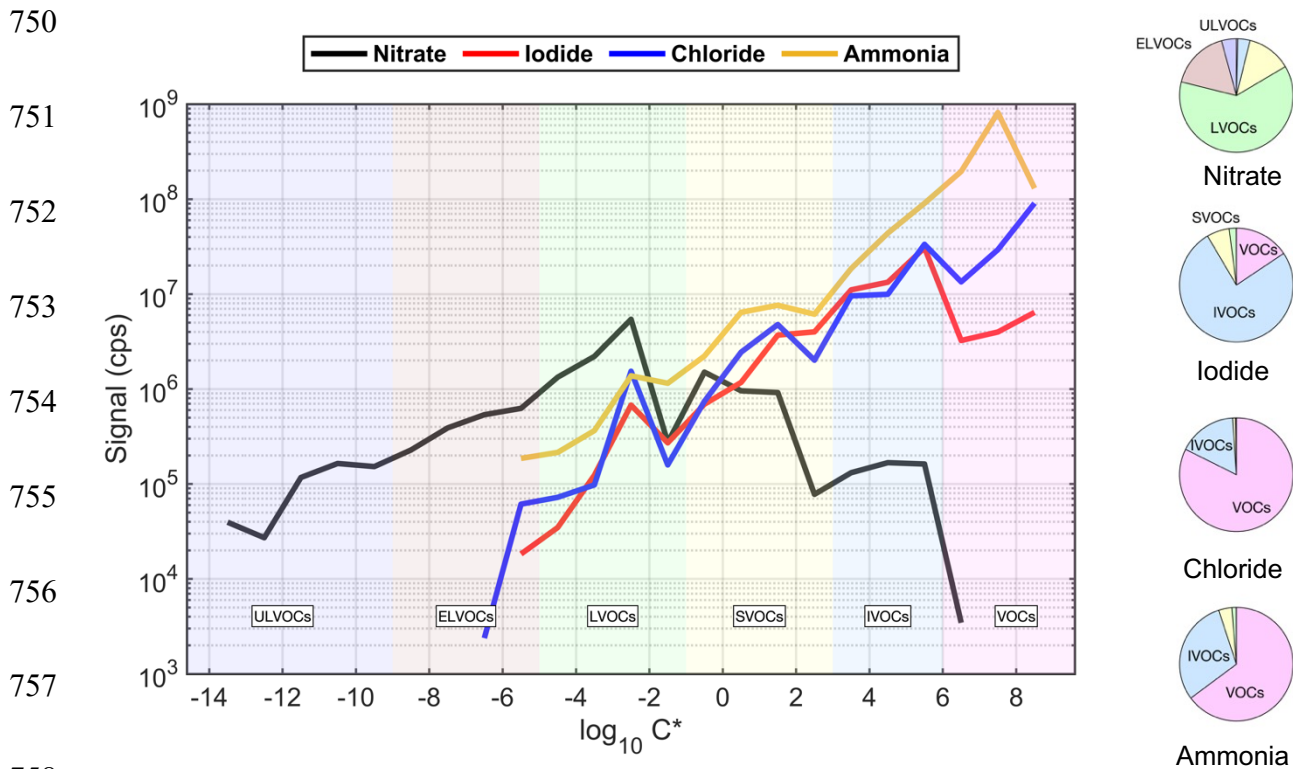
Figure 6. Volatility distribution comparison for organic compounds detected by the Vocus AIM using nitrate, iodide, chloride, and ammonia ion chemistries. Ion intensity represents the cumulative signal recorded for each ion chemistry. The background colors represent the saturation concentration (C_{sat}) in the range of ultra-low volatility (ULVOCs), extremely low volatility (ELVOCs), low volatility (LVOCs), semi-volatile (SVOCs), intermediate volatility (IVOCs), and volatile organic compounds (VOCs, pink). The pie charts represent the corresponding contributions of VOC, IVOC, SVOC, LVOC, ELVOC, and ULVOC classes from the O_3/OH initiated oxidation of α-pinene.